N92-21885

COMPTEL: instrument description and performance

J.W. den Herder[2], H. Aarts[2], K. Bennett[4], H. de Boer[2], M. Busetta[4], W. Collmar[1], A. Connors[3], R. Diehl[1], W. Hermsen[2], J. Ryan[3], M. Kippen[3], L. Kuiper[2], G. Lichti[1], J. Lockwood[3], J. Macri[3], M. McConnell[3], D. Morris[3], R. Much[1], V. Schoenfelder[1], G. Stacy[3], H. Steinle[1], A. Strong[1], B. Swanenburg[2], B.G. Taylor[4], M. Varendorff[1], C. de Vries[2], C. Winkler[4]

[1] Max-Planck Institut fuer extraterrestrische Physik, D-8046 Garching, FRG
[2] Laboratory for Space Research Leiden, POB 9504, 2300 RA Leiden, The Netherlands
[3] University of New Hampshire, Institute for the Studies of Earth, Ocean and Space, Durham NH 03824, USA
[4] Astrophysics Division, Space Science Department of ESA/ESTEC, NL-2000 AG Noordwijk, The Netherlands

Abstract

The imaging Comtpon telescope, COMPTEL, is one of the four gamma-ray detectors onboard of the Compton Gamma-Ray Observatory (GRO). COMPTEL is sensitive to gamma-rays from 800 keV to 30 MeV with a field of view of approximately 1 sr. Its angular resolution (1 σ) ranges between 1° and 2° depending on the energy and incident angle. The energy resolution of better than 10% FWHM enables COMPTEL to provide spectral resolution in the regime of astrophysical nuclear lines. The effective area (for normal incidence) varies typically between 10 and 50 cm^2 depending on the energy and event selections made. In its telescope mode COMPTEL is able to study a wide variety of objects, pointlike as well as extended in space. With 0.125 msec timing resolution, pulsed emission can be studied. In single detector mode COMPTEL uses two of its detectors to study the temporal spectral evolution of strong gamma-ray bursts or transients.

A short description of the intrument, its characteristics as deduced from calibration measurements and simulations, and some first results on the inflight performance are presented.

Introduction

The exploration of the sky for gamma-ray energies between 1 and 30 MeV lags far behind the exploration in the X-ray band and at higher gamma-ray energies. Apart from a limited number of balloon flights, this energy range has hardly been explored. In this energy region an important interaction mechanism is Compton scattering. The photo-electric absorption cross section falls above 100 keV while pair production becomes significant above about 40 MeV. Photons between 1 and 30 MeV, including that part of the spectrum which is rich in nuclear lines, are very penetrating and can propagate over large distances in the universe carrying information about their origin. At the same time, this property makes it very hard to detect and measure them. In addition the showering activity of photons and electrons as well as de-excitation of atomic nuclei, cause a very high background in this energy band explaining its rather unexplored nature.

Inevitably, an imaging detector covering this energy range may rely on the Compton interaction. In this type of detector two detector layers are used. In the first layer (D1) the incoming gamma ray is subject to a Compton interaction and the scattered gamma is, idealistically, completely absorbed in the second layer (D2). In this case the Compton scatter kinematics (eq. 1) yield the scatter angle ($\bar{\phi}$) of the incoming gamma ray and thus defines, combined with the location of the interactions in both detectors, a circle at the sky.

$$\bar{\phi} = \arccos(1 - E_e/E_2 + E_e/(E_1+E_2)) \qquad (1)$$

where $E_\tau = E_1 + E_2$ is the energy of the incoming gamma ray, E_1 and E_2 are the energy deposits in the upper and lower detectors respectively and $E_e = m_e c^2$.

In figure 1 a schematic drawing of COMPTEL is given showing the main detector components (some of the key parameters are listed in table 1, see also reference 1). The upper detector consists of 7 liquid scintillators (NE 213A), the lower detector of 14 NaI scintillators. Each detector is monitored by a number of photo multiplier tubes (PMT). Time-of-flight measurement allows to discriminate forward moving gamma rays from backward moving gamma rays, reducing the background significantly. Each detector plane is surrounded by two anticoincidence shields rejecting charged particles. Neutrons, not detected by the anticoincidence shields, are rejected using pulse shape discrimination techniques in the D1 detector. Finally the figure shows clearly some of the mechanical structure around the D1 and above the D2.

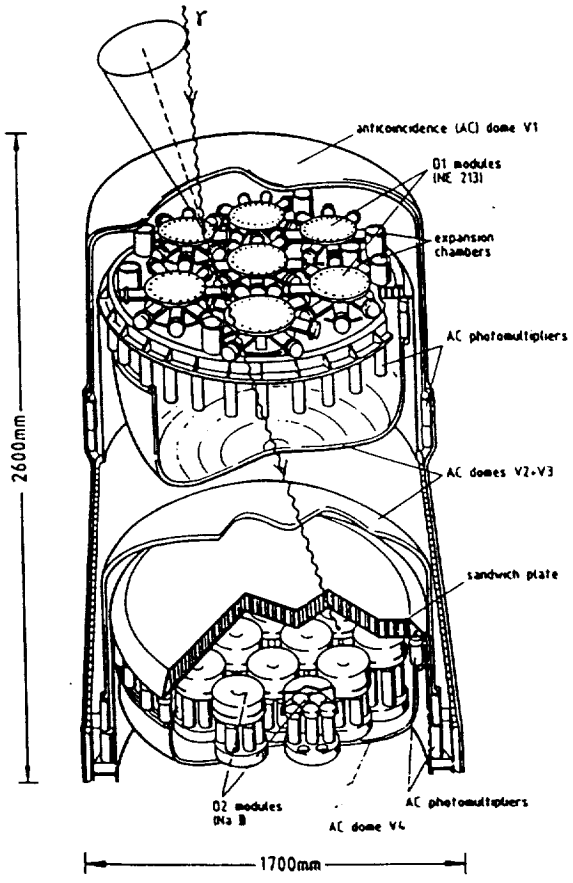

fig. 1 Cut away schematic of COMPTEL.

For each gamma-ray event, which is electronically defined by a delayed coincidence between the upper and lower detector in absence of a veto signal from the anti-coincidence shields the following quantities are available:

Table 1 Some key parameters

D1	: NE 213A, 4188 cm^2
D1 energy	: 50 keV - 20 MeV
D2	: NaI, 8620 cm^2
D2 energy	: 500 keV - 30 MeV
Energy	: 0.720 - 30 MeV, resolution 5-8% (FWHM)
$\bar{\phi}$	: angular resolution 1.7° - 4.4°
A_{eff}	: 20 - 50 cm^2
FoV	: 1 sr
timing	: 1/8 msec

- energy deposit in the upper detector
- location in the upper detector
- pulse shape in the upper detector
- energy deposit in the lower detector
- location in the lower detector
- time-of-flight between the upper and the lower detector
- the absolute time of the event

The pulse-shape and time-of-flight information are used to optimize the signal to noise ratio. The two interaction locations define, together with the pointing of the instrument a point at the sky and the two energy deposits can be converted into the Compton scattering angle ($\bar{\phi}$). This relation (see also eq. 1) is visualized in fig. 2. As a function of the energy deposit in the D1 and the D2 lines of equal E_τ and of equal $\bar{\phi}$ are drawn. The field of view is limited by the hardware energy thresholds: the E_1 threshold determines the lower range in $\bar{\phi}$ and the E_2 defines the upper range.

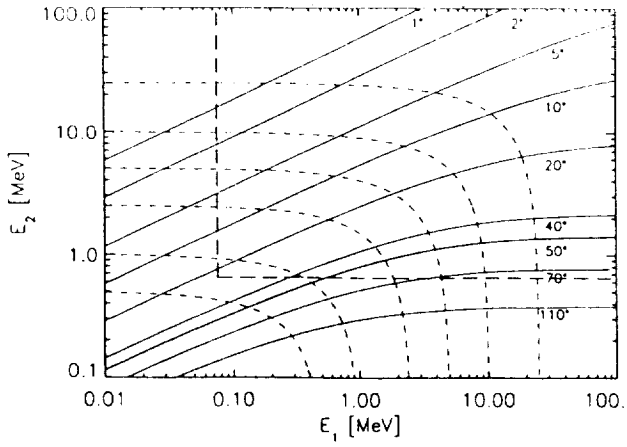

fig. 2 Relation between E_τ, E_1, E_2 and $\bar{\phi}$ for totally absorbed events.

In fig. 3 the Compton scattering cross section according to the Klein-Nishina formula is given for different energies. The probability for a Compton scatter decreases with increasing energy. The relative probability for a Compton scatter angle of less than 50° is indicated. This corresponds roughly to the applied selection in the present analysis (see also fig. 2). As can be noticed about half of the events have a scattering angle of less than 50°.

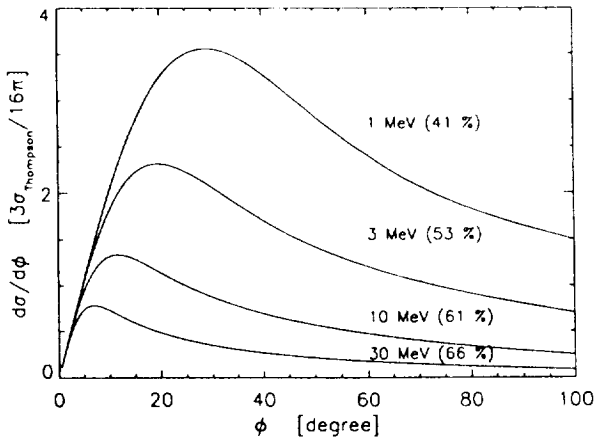

fig. 3 Klein-Nishina cross section for different energies (the relative probability for a scatter angle of < 50° is indicated between brackets).

The COMPTEL response is characterized by a cone with half-opening angle of 45° (see fig. 4) and a distribution along the cone given by the Klein-Nishina formula. The width of the response cone is given by the limited energy and interaction location resolution within the detector modules. Incompletely absorbed events in the D2 populate the inner part of the cone (see Diehl et al., these proceedings).

The width of the cone is a measure for the angular resolution of COMPTEL. In fig. 5 this is shown in a 2-dimensional representation. When no background is present all source events should be concentrated around $\bar{\phi} - \phi_{geo} = 0$ where ϕ_{geo} is the true scattering angle knowing the position of the (calibration) source. This quantity is referred to as Angular Resolution Measure (ARM=$\bar{\phi} - \phi_{geo}$). Partially absorbed events in the D2 will shift to larger $\bar{\phi} - \phi_{geo}$ values. In flight, however, the distribution will be dominated by background events and only strong sources will be identified by a clear signature in the ARM distribution.

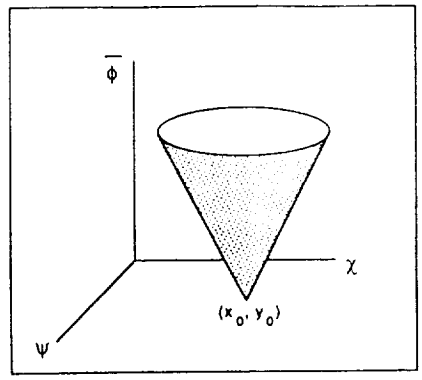

fig. 4 Schemical response of COMPTEL to a point source at position (x_o, y_o).

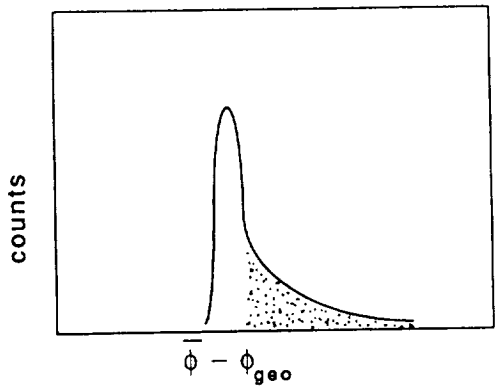

fig. 5 Schematical ARM distributions for a source at a know position (the shaded area indicates not fully absorbed events in the D2)

Main detector elements

The material used for the D1 is a liquid organic scintillator, NE 213A, with low density and low Z in order to maximize the probability of a single Compton interaction. The energy response of this detector is well described by a single Gaussian ($1\sigma = 1.10E^{0.57}$ where the energy is in keV) covering an energy range from 50 keV to 20 MeV. Each D1 detector is monitored by 8 PMTs. Using the Anger camera principle and a neural-net method[2] a spatial resolution of 2.3 cm (1σ) is obtained. The total geometric area for the 7 D1 modules is 4188 cm^2. The D1 also displays pulse shape discrimination properties. This allows to discriminate the slower rise times of proton ionization tracks, caused by neutron scattering on hydrogen, from the short rise times caused by electrons and other minimum ionizing particles. This pulse shape discrimination (PSD)

capability is shown in fig. 6 where the neutrons can be clearly separated from the gammas (note that the curved energy/PSD relation is made linear in the analysis). Alternatively this capability to distinguish neutrons and gammas can be used to measure neutrons created in solar flares (see Ryan et. al., these proceedings).

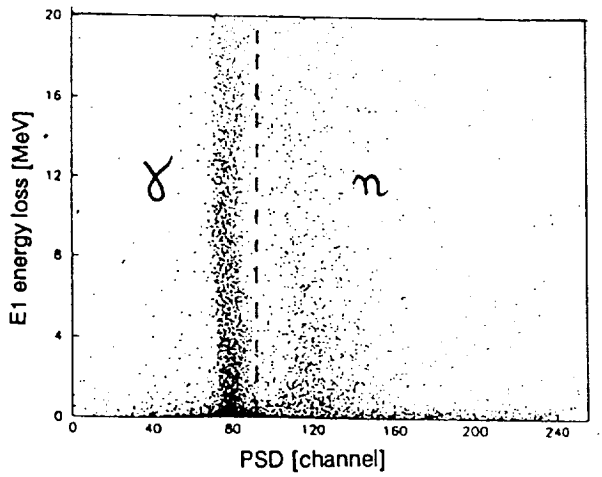

fig. 6 Pulse shape discrimination capability of COMPTEL.

For the D2 detectors NaI was selected to optimize photopeak efficiency. A typical spectrum is shown in fig. 7 where the different components (photo-peak, 1st and 2nd escape peaks and Compton edge) are clearly indicated. The energy resolution, up to 6.1 MeV, is well described by the square-root law ($=1.719E^{0.5}$ - 11.8, E in keV). Above this energy the photopeak signature in the data is not evident anymore. These detectors cover roughly an energy range from 0.6 to 30 MeV.

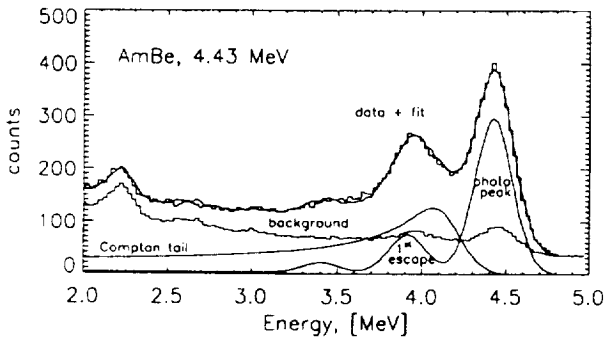

fig. 7 A D2 energy spectrum for AmBe (4.43 MeV). The various components are all indicated.

Each D2 detector is monitored from underneath by 7 PMT's. Using the Anger camera principle, the typical spatial resolution is 2.4 cm. In fig. 8 the spatial resolution for a single module is shown. The total geometrical area is 8620 cm^2.

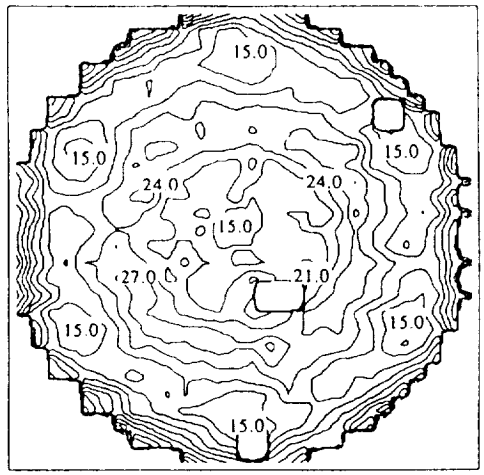

fig. 8 A D2 1-σ event location contour map for a single module (resolution in mm, radius ~ 140 mm).

Apart from the double scatter mode, two D2 modules are operated in single detector mode upon receiving a trigger from BATSE (the Burst and Transient Experiment onboard GRO)[3]. The electronics of these two modules are optmized to cover two different energy regions (0.1 - 1.1 MeV and 1 - 10 MeV respectively) and the time evolution of burst events can be recorded.

Other main detector features include:
- time-of-flight measurement between the upper and lower detector planes (separated by 1.58 m). The time-of-flight is measured with a 3 ns accuracy;
- the rejection of charged particles by the anti-coincidence shields (>99.9 % for each anti-coincidence shield);
- two ^{60}Co doped scintillators, mounted halfway between the D1 and the D2 (CAL units). ^{60}Co emits simultaneously 2 gamma rays (1.17 MeV and 1.33 MeV). These gamma rays are used to monitor the PMT gains and to determine the appropriate corrections;
- accurate measurement of the arrival time of each gamma (0.125 msec accuracy) allows for timing analysis of fast pulsars.

Instrument characteristics

For an imaging telescope the critical parameter is the point spread function which has been determined using different methods, namely[4]:
- measurement of the telescope response using a number of known calibration sources at different orientations with respect to COMPTEL;
- measurement of the single detector responses and calculating the telescope response using this single detector response and the known properties of the Compton scatter interaction;
- Monte Carlo simulation of the response for a given source position and input spectrum.
In figure 9 the measured response is shown for three energies.

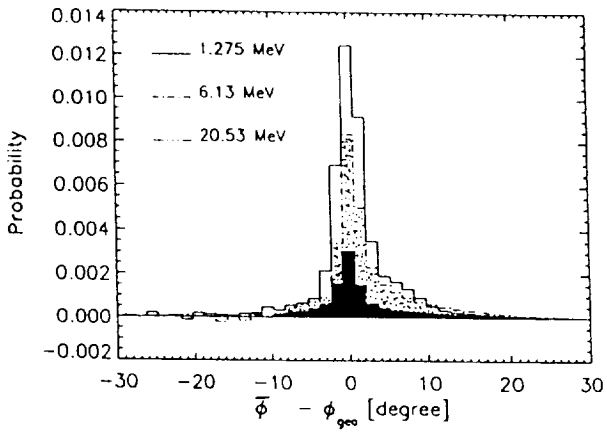

fig. 9 ARM distribution for three different input energies (black area = 20.52 MeV, dotted area = 6.13 MeV, empty area = 1.275 MeV).

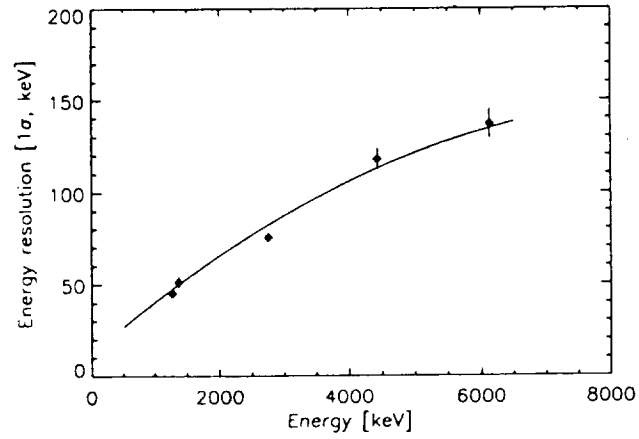

fig. 10 Telescope energy resolution based on calibration measurements (data) and on Monte Carlo simulations (line).

In figure 10 the energy resolution as a function of energy is shown. An energy resolution of better than 10% FWHM enables COMPTEL to provide spectral resolution in the regime of nuclear lines.

In fig. 11 the angular resolution is given. At energies above about 2 MeV the angular resolution is dominated by the D1 and D2 location uncertainty while, at lower energies, the energy resolution predominantly determines the angular resolution per the Compton scatter formula.

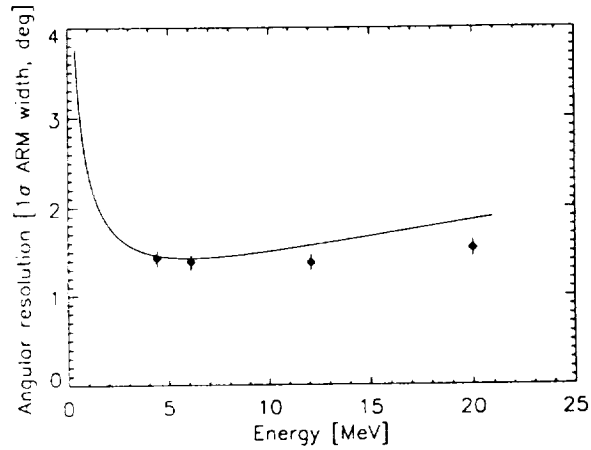

fig. 11 Telescope angular resolution as determined for calibration measurements (data) and from Monte Carlo simulations (line).

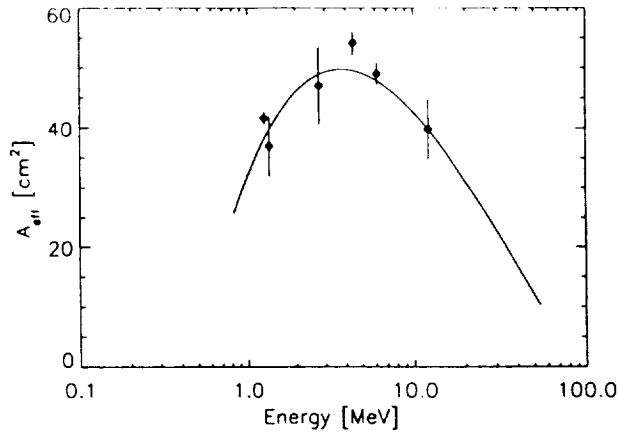

fig. 12 Effective detection area for normal incidence as deduced from calibration measurements (data) and Monte Carlo simulations (line).

In figure 12 the effective sensitive area of the telescope is given for vertical incidence as deduced from the calibration measurements. These results include the effects of the time-of-flight and PSD

selections as well as energy thresholds in the D1 and D2 of 50 and 500 keV, respectively (somewhat lower than the present in flight values). Further selections on the data (such as selection of photo-peak events only) typically reduce the effective area by a factor 2.

Obviously, the effective area depends on the incidence angle as well. This is demonstrated in figure 13 for 1.275 MeV. At higher energies the fall off is somewhat steeper than at 1.275 MeV.

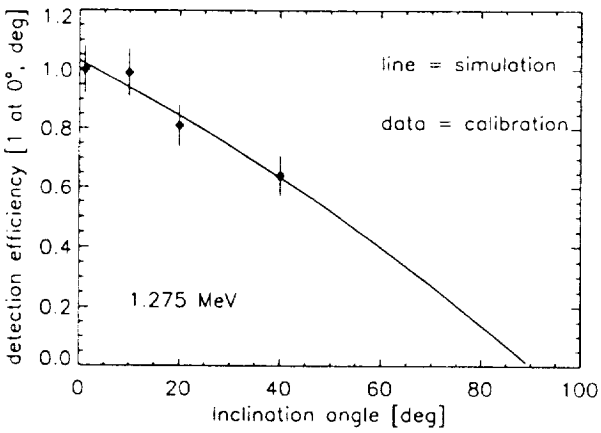

fig. 13 Detection efficiency as a function of inclination angle.

The energy response of the burst modules was calibrated separately before and after integration of COMPTEL on the Observatory. This was required since the response of these modules, which are in principle 4π sensitive, depends heavily on the position of the burst due to the large differences in absorbing material on the spacecraft. For this reason, the burst response decreases dramatically for incidence angles larger than 60°.

Operational modes

The main operational modes include the following:

Double scatter telescope mode:
In this mode a gamma event is defined by a coincidence between the upper and the lower detector in the absence of a signal in the anti-coincidence shields. The onboard selection includes a time-of-flight selection and energy threshold selections. Events with a time-of-flight value between - 7ns and +8 ns with respect to forward scattered gamma events and D1 and D2 energies larger than 65 keV and 600 keV, respectively, are selected (the gamma-1 class). In addition a subset of events with lower energies (larger than 35 and 440 keV respectively) or a less strict window on the time-of-flight (-23 ns to 20 ns) are selected for background studies (gamma-2 class). The available telemetry is first used to transmit gamma-1 events and any remaining capacity is used to transfer the gamma-2 events.

Single detector mode (burst mode):
The burst mode of the two D2 modules is triggered by the BATSE instrument onboard GRO. In absence of a BATSE trigger background spectra are accumulated (2-512 sec telecommandable integration time). After receipt of a BATSE trigger 6 high time-resolution burst spectra are recorded (0.1-25.6 sec telecommandable integration time). Following these 6 burst spectra up to 255 'tail' spectra can be collected (2-512 sec integration time) before the electronics return to the background mode. Gamma-ray bursts, occurring in the field of view and of sufficient strength are, of course, also recorded in the 'double scatter mode'. Then these bursts can be located on the sky with a typical accuracy of less than 2°, using the imaging capability of COMPTEL.

Solar neutron mode:
When BATSE records a burst in the direction of the sun, COMPTEL will switch to the 'solar neutron mode'. In this operational mode events continue to be recorded in the double scatter telescope mode. In addition the 'single detector mode' is enabled to record the evolution of the gamma-ray spectra. Finnally the selections of the gamma-2 channel, usually used for background monitoring, are optimized for the detection of neutrons by shifting the onboard time-of-flight selection to -10 to +33 ns. This enables the recording of neutrons down to about 10 MeV.

Special modes:
There are a number of special modes which support the routine operations. These include the 'proton mode' (no anti-coincidence with the veto shields), the 'D1 single mode' (no coincidence with a D2 trigger), the 'D2 single mode' (no coincidence with a D1 trigger), the 'SAA mode' (a high rate for the light emitting diodes which are attached to each detector module) and an 'atmospheric neutron mode' (settings optimized to detect atmospheric neutrons).

Inflight performance

Since the launch of GRO on April 5th, 1991, and the subsequent checkout and tuning of the instruments COMPTEL has behaved rather stably with two exceptions:
- Module D2-14 appeared to have a noisy PMT since May 24th, 1991, and had to be turned off for that reason;
- Module D1-4 showed high voltage loading problems since July 3rd, 1991, and is also turned off.
Effectively this reduces the telescope efficiency to about 80%. Unfortunately module D2-14 served also as the low-energy burst detector and thus only the high-energy burst detector remains operational.

Each day COMPTEL experiences up to 9 passages through the South Atlantic Anomaly (SAA) during which the high voltages are switched off (about 10% of the observation time). As a consequence of the fixed pointing at the sky during a two week observation the effective viewing time is further reduced to about 30% by the earth blocking the field of view. During each day about 600.000 gamma-1 events are recorded. In the standard analysis about 2/3 is rejected based on the time-of-flight values, the pulse shape information and the energy threshold of the modules. Of the remaining events about 20% is rejected since the scatter angle is larger than 50° and about 40% of the then remaining events are coming from the earth. Finally about 80.000 events remain for further analysis. This number includes events from gamma-ray sources, from the galactic and extra-galactic background, but also includes a substantial contribution from the instrumental background.

In figure 14 orbital variations for a number of characteristic parameters are displayed. On the top panel the high voltage (HV) of the D1-1 module is shown. The different SAA passages can be clearly identified. At the second panel the gamma-1 + gamma-2 rate is given. During SAA passages these rates drop to zero. In addition there are large fluctuations correlated with the cut-off rigidity (given at the bottom). The third panel displays the gamma-1 rate and the fourth panel the high-range burst detector rate, both correlate with rigidity. In the second lowest panel the veto rates are shown.

As stated, the instrumental background varies heavily as a function of geomagnetic latitude. This is demonstrated in figure 15 where the gamma-1 rate is plotted versus cut-off rigidity. The two branches in this correlation plot correspond to the time the earth is in the field of view (top branch) and the time COMPTEL is looking to the sky (lower branch). Even when looking to the sky the variations in the instrumental background vary by at least a factor 2 over the orbit.

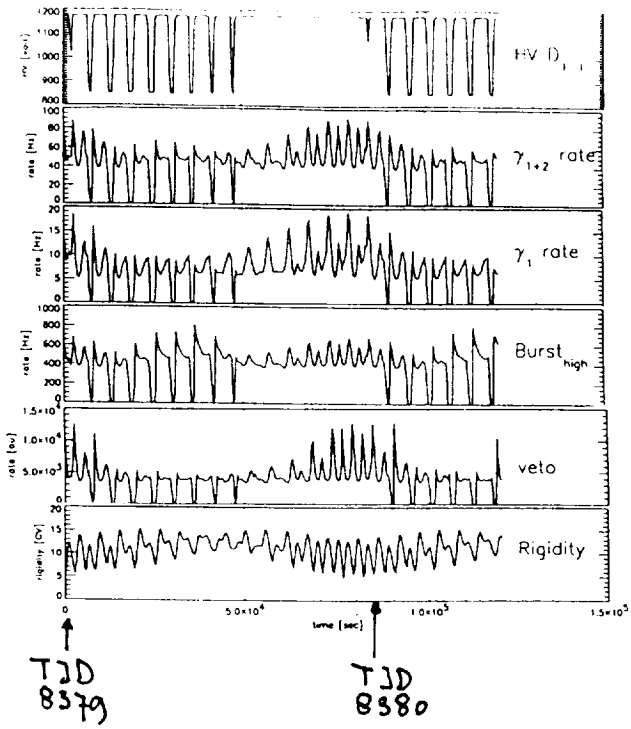

fig. 14 Typical orbital variations (see text for more details).

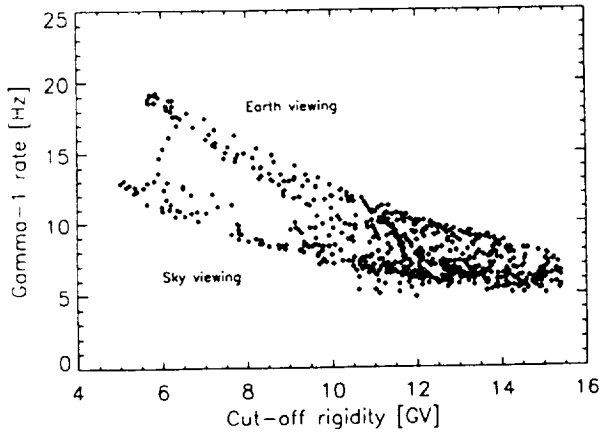

fig. 15 Gamma-1 rate as a function of rigidity.

In figure 16 a time-of-flight spectrum is shown, integrated over a full day and selecting periods of the orbit when the earth is not in the field of view. As expected the relative number of forward scattered events decreases if earth-viewing parts of the orbit are rejected (since the earth is a very strong source of gamma-rays). In the bottom panel of fig. 16 ϕ distributions for three typical time-of-flight selections are shown. The central lower panel corresponds to forward scattered events and could, in first order, be compared with the Klein-Nishina distributions shown in fig. 3. The two other panels show the ϕ distributions of background components. The left panel contains events with lower time-of-flight values. These so-called 'cascade' events are produced by the interaction of energetic cosmic rays with the spacecraft. The right panel is illustrative for the level of accidental coincidences and the $\bar{\phi}$ distribution is very similar to the interaction probability as determined by the geometry of COMPTEL.

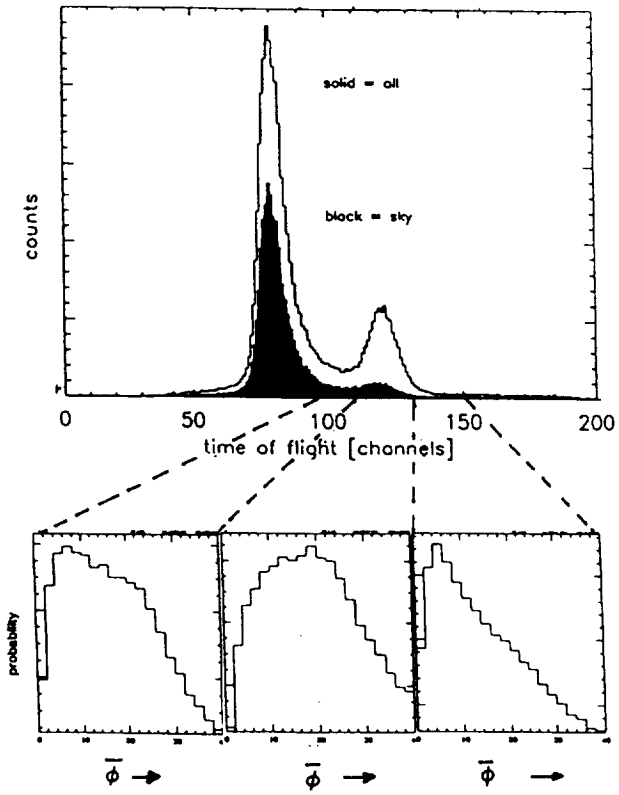

fig. 16 Time-of-flight distributions for a full day (line) and for the earth-viewing part of the orbit (solid). $\bar{\phi}$ distributions for different ToF windows are given.

As part of the in flight tuning the energy thresholds were set, since these directly affect the field of view.

In fig. 17 and 18 the thresholds for two D1 and two D2 modules are shown. The setting of thresholds is performed in three steps:

- onboard, a hardware threshold is set below which no trigger is accepted. This threshold can be set individually for each module (in the D1) or in pairs (in the D2). Due to different gains the corresponding energy of each hardware threshold differs.
- a software threshold is set as part of the onboard selection of gamma-1 events. Only one software threshold is available for the entire D1 and one for the entire D2 and these are applied on the raw data before these are corrected for gain fluctuations in the PMT s.
- finally in the analysis a software threshold is applied to the events after corrections have been applied for fluctuations in the PMT gains. This threshold is the same for all D1 and all D2 modules. It should be set sufficiently high to exclude variations in the effective area due to fluctuations in the gains.

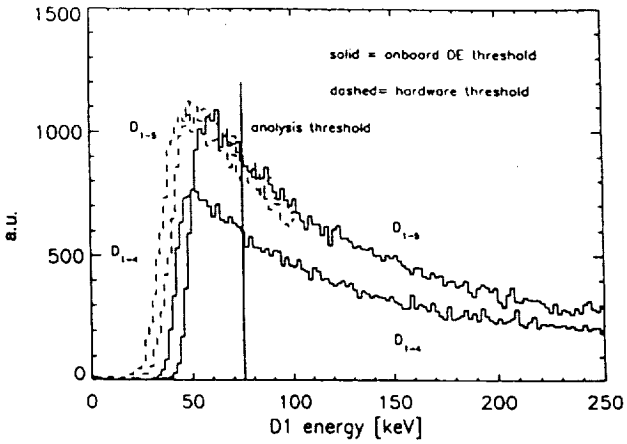

fig. 17 D1 energy thresholds for two modules. The dashed curve represents the effect of the onboard hardware threshold, the solid curve represents the effect of the onboard set software threshold and the straight line is illustrative for the threshold set during analysis of the data.

The onboard threshold and the analysis threshold of the D2 was set to about 580 keV and 650 keV respectively in order to reduce the very strong instrumental 511 keV line due to β^+ decay of the activated ^{11}C in the D1 detectors. A remainder of this 511 line can still be seen in the hardware threshold curve in fig. 18.

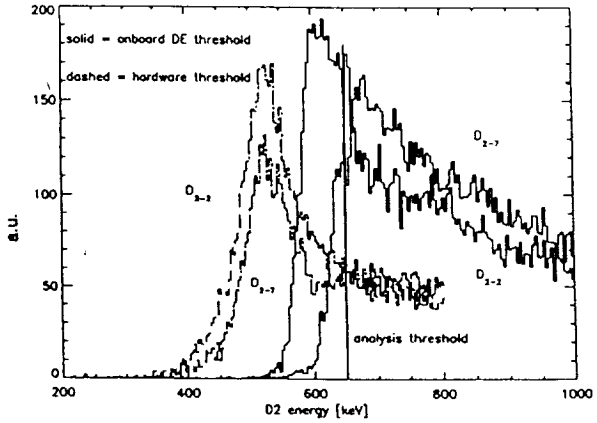

fig. 18 D2 energy threshold (for caption see fig. 16).

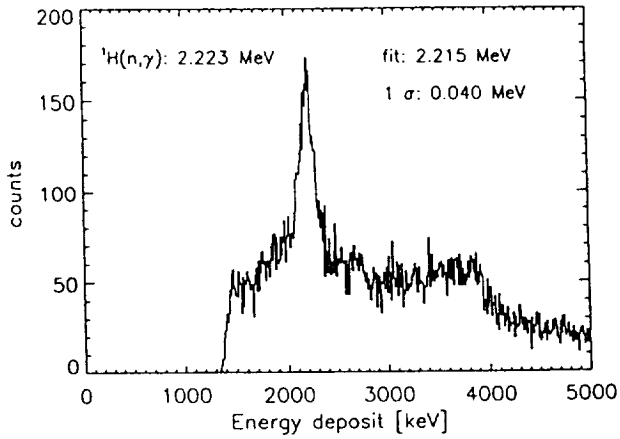

fig. 19 Total energy spectrum of the 2.223 MeV instrumental background line.

The in-flight energy calibration depends heavily on the corrections made for the gain fluctuations in the PMTs. These gains may fluctuate up to 40% for an individual PMT and, although not systematically, show largest fluctuations immediately after a SAA. On average the gains increased by about 10% compared to the pre-flight calibration measurements. While the D2 energy calibration and gain corrections could easily be verified by the photopeak signatures of the 1.17 and 1.33 MeV gamma rays from the two ^{60}Co doped calibration units, this is less straight forward for the D1 modules since these show only a broad Compton distribution for these events. The D1 energy calibration could, however, be checked independently using the neutron capture line of 2.223 MeV in hydrogen. In fig. 19 the result of this check is demonstrated and there is excellent agreement.

Finally the inflight performance of COMPTEL was evaluated during the initial period in orbit by pointing towards the Crab Nebula. In figure 20 the ARM distribution for a one day pointing is shown and the source signature is clearly seen on top of the background. The fact that it is nicely concentrated around 0° is a demonstration of the correct in-flight energy calibration. The estimated systematic error on the position is less than 0.5°. The in-flight sensitivities will be reported elsewhere in these proceedings (see Schoenfelder et al., these proceedings).

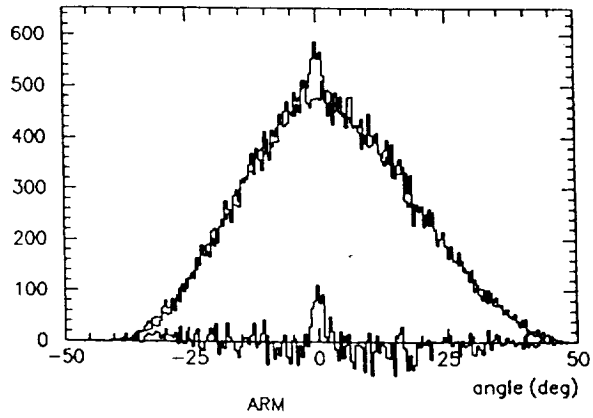

fig. 20 ARM distribution for a one day observation on the Crab Nebula. The lower histogram displayes the difference between the ARM distribution for the Crab Nebula and the background estimate for that observation.

Conclusion

It has been demonstrated that COMPTEL performs well in orbit and that most orbital variations in the data are under control which reduces systematic uncertainties in the data to a minimum. Nevertheless the results of COMPTEL will depend heavily on our detailed understanding of the background and this work could only start after launch (see Diehl et al., these proceedings).

References

[1] V. Schoenfelder et al., IEEE Trans on Nucl. Sci., NS-31, No 1, 766-770, (1984)

[2] A. Connors et al., Neural net approaches for event location in the detector modules, in Data Analysis in Astronomy IV, Erice, Italy 1991, in print

[3] C. Winkler et al., Observing cosmic gamma-ray bursts with COMPTEL, in proceedings of GRO science workshop, Greenbelt MD, USA, 1989

[4] R. Diehl et al., Response Determinations of COMPTEL from Calibration measurements, Models and Simulations, in Data Analysis in Astronomy IV, Erice, Italy 1991, in print